Sensitivity of Polarimetric and Interferometric Phases to Ice Sheet Subsurface Density

Georg Fischer [a], Konstantinos Papathanassiou [a], Irena Hajnsek [a,b]
[a] German Aerospace Center (DLR), 82234 Wessling, Germany
[b] ETH Zurich, 8092 Zurich, Switzerland

Abstract

The subsurface density of ice sheets is a key uncertainty in mass balance estimations. Synthetic Aperture Radar (SAR) measurements of polarimetric and interferometric phases contain information about the density, but were only considered separately. Polarimetric phases are related to the dielectric anisotropy of firn, but multiple incidence angles are required to solve for density and a quantitative sensitivity analysis is missing. Interferometric phases were used to retrieve densities in tower-based SAR tomography experiments, requiring large incidence angle variety and high resolution. This study conducts a combined sensitivity analysis of polarimetric and interferometric SAR measurements towards a density retrieval.

1 Introduction

A key uncertainty in mass balance studies of glaciers and ice sheets is still today the density for the volume-to-mass conversion. This is not only reported on a global scale [1] but also for recent local studies [2], where even the presence of in situ measurements can only partly capture the density uncertainty [3]. The volume-to-mass conversion factor can span a wide range from 0 to 2000 kg m^{-3} but many studies use fixed density values such as 850 ± 60 kg m^{-3} [4]. Therefore, there is a clear need for improved spatial and temporal information about ice sheet subsurface properties such as the density.

Synthetic Aperture Radar (SAR) is promising for this task due to the penetration of the microwave signals of several tens of meters into dry snow, firn and ice, particularly at longer wavelengths such as L or P band [5], and their sensitivity to subsurface properties. Also its large spatial coverage and high resolution could improve existing model- or in situ-based subsurface density information.

A promising information lies in phase measurements of coherent SAR. Interferometric (InSAR) phase differences provide information about the location of scatterers in the subsurface. The decorrelating nature of phase contributions from different depths leads to the key InSAR observable of volume coherence, which can be related to subsurface structure. Another phase difference, between polarimetric channels (PolSAR), can be related to the dielectric anisotropy of snow and firn and is thus sensitive to wave propagation properties in the subsurface.

To name some examples, (Pol-)InSAR volume decorrelation can indicate subsurface properties about refrozen melt layers [7] and signal extinction [8]. With multi-baseline InSAR data, tomographic 3D-imaging (TomoSAR) of the subsurface is possible and subsurface layers, different ice types, firn bodies, and crevasses were identified [9][10][11]. Polarimetric phase differences, i.e. the co-polarization HH-VV phase difference (CPD), were linked to firn thickness by assuming bulk values for density and anisotropy and employing a constant signal extinction for the vertical backscattering function [12].

Despite the promising information content of these phase-based SAR measurements, a key ambiguity remains between the depth of scatterers and the permittivity of the medium, which this study addresses. The translation of an interferometric phase, or similarly the depth-axis of a tomogram, into its actual depth below the surface depends on the permittivity of the snow, firn and ice. The permittivity is given by the density of the medium [13]. Also the polarimetric HH-VV phase difference, the CPD, for a given anisotropic propagation in the subsurface, depends on the density, albeit differently than the interferometric phase.

One way of addressing the density-dependence of such phase measurements is therefore the combination of interferometric and polarimetric phase measurements. A second way is the exploitation of different incidence angles, because of the permittivity-driven, and thus density-related, refraction.

This second aspect was already addressed in several studies for ground-based interferometric or tomographic measurements where the density ambiguity can be solved with measurements at different incidence angles [14][15][16]. However, a large incidence angle variation and a high resolution is required for a precise location of scatterers, which is challenging for spaceborne concepts [17].

This study addresses the combination of PolSAR and InSAR, by investigating the sensitivity of interferometric and polarimetric phase-based measurements to ice sheet subsurface density. Further, the influence of the incidence angle will be analyzed, as measurements with at least two incidence angles are required to solve for density also in this case. The results will describe a potential way towards a density retrieval from multi-angular Pol-InSAR data.

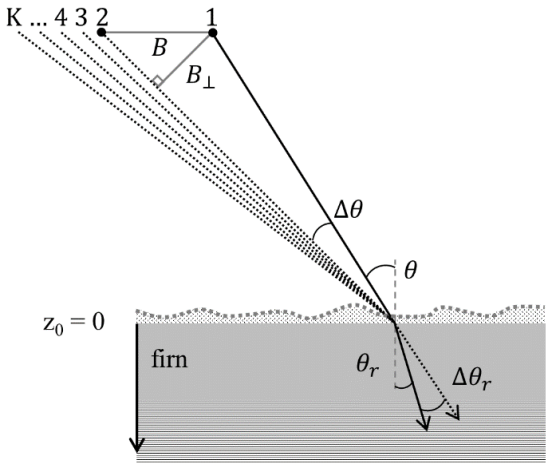

Figure 1 Multi-baseline interferometric geometry with K acquisitions, perpendicular baseline $B_\perp$, incidence angle in air θ and the refracted incidence angle in the snow, firn or ice volume θ_r.

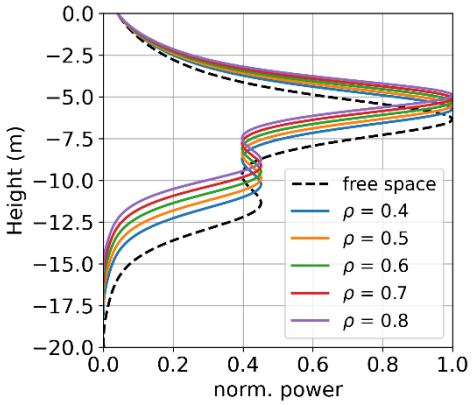

Figure 2 Example of a real TomoSAR profile in L-band from the South Dome location in Greenland showing the effect of two distinct refrozen melt layers within the firn subsurface. The colours indicate different density assumptions and show its effect on the translation of (multi-baseline) interferometric phases to depth.

2 Methods

2.1 Density dependence of the interferometric phase

In the fields of InSAR and TomoSAR for the investigation of the ice sheet subsurface, recent studies are mainly concerned with the estimation of the vertical backscatter distribution, either with (Pol-)InSAR structure models or through tomographic imaging techniques. The fundamental interferometric observable is the coherence, which describes the complex correlation between two SAR measurements separated by a spatial baseline, see **Figure 1**. After compensating or neglecting range spectral and noise decorrelation terms, the main contribution is the volume coherence γ_{Vol}

$$\gamma_{Vol} = e^{ik_z z_0} \frac{\int_{-\infty}^{0} \sigma(z) e^{ik_{zVol} z} dz}{\int_{-\infty}^{0} \sigma(z) dz}. \quad (1)$$

It depends on the vertical backscatter distribution in the subsurface $\sigma(z)$ and on the vertical wavenumber k_{zVol} which is the phase-to-height conversion factor, defined by the interferometric acquisition geometry in **Figure 1**

$$k_{zVol} = \frac{4\pi\sqrt{\epsilon_r}}{\lambda} \frac{\Delta\theta_r}{sin\theta_r} = k_z \sqrt{\varepsilon_r} \frac{cos\theta}{cos\theta_r}. \quad (2)$$

The vertical wavenumber in the volume k_{zVol} considers the difference between the real depth of a scatterer within the subsurface and its apparent position, if processed under the assumption of free-space propagation, by accounting for the permittivity ε_r of the medium. A scatterer at an apparent depth d_{app} in free-space processing has a real depth d

$$d = d_{app} \frac{cos\theta_r}{\sqrt{\varepsilon_r}\, cos\theta} \quad (3)$$

See also the equivalent derivation in [18]. Assuming that a specific scatterer can be located in the snow, firn or ice through an InSAR measurement, its real depth d cannot be determined unambiguously as long as $\sqrt{\varepsilon_r}$ is unknown.
This is shown for a vertical profile $\sigma(z)$, derived with TomoSAR processing at L band, in **Figure 2**, where the effect of two distinct refrozen-melt layers within the firn subsurface of Greenland is visible at about -5 m and -10 m [19]. The colours show the same profile processed with different density assumptions, which lead to different permittivities and thus k_{zVol}.

2.2 Density dependence of the polarimetric phase difference

In the field of PolSAR, modeling efforts have been dedicated to establish a link between measured co-polarization (HH-VV) phase differences (CPD)

$$CPD = \angle(s_{HH}\, s_{VV}^*) = \phi_{HH} - \phi_{VV} \quad (4)$$

and the anisotropic structure of firn originating from temperature gradient metamorphism [20].
CPDs have then been modeled as the result of birefringence due to the dielectric anisotropy $\Delta\varepsilon = \sqrt{\varepsilon_H} - \sqrt{\varepsilon_V}$.

$$CPD = \angle\left\{\int_{-\infty}^{0} \sigma(z) e^{2j\frac{2\pi}{\lambda_0}(\sqrt{\varepsilon_H}-\sqrt{\varepsilon_V})\frac{z}{\cos\theta_r}} dz\right\} \quad (5)$$

The dielectric anisotropy, i.e. $\sqrt{\varepsilon_H}$ and $\sqrt{\varepsilon_V}$, can be modelled from an ice-air mixture of density ρ consisting of spheroidal ice particles with a certain axial anisotropy DA (Degree of Anisotropy), resulting in $\varepsilon_{H,V} = f(\rho, DA)$ [20]. Typical values for the dielectric anisotropy of firn are $0.02 < \Delta\varepsilon < 0.07$ [21].
In addition, the relation between the anisotropic signal propagation and measured CPDs depends on the vertical distribution of backscattering $\sigma(z)$ in the subsurface, which defines how the CPD contributions are integrated along depth and thus $CPD = f(\sigma(z), \rho, DA)$.

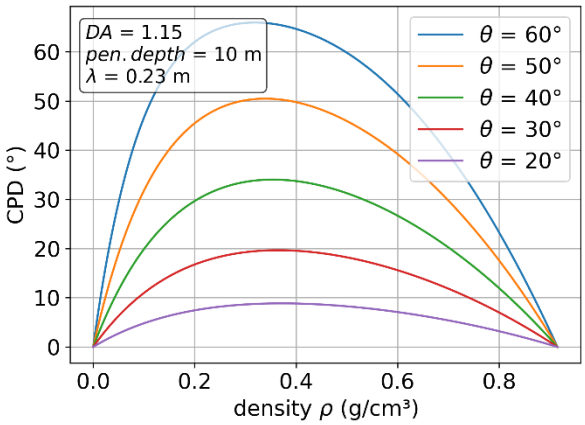

Figure 3 Modelled CPD for an L-band wavelength as a function of density, for a 10 m one-way penetration depth in anisotropic firn with an axial ratio of the modelled firn grains of 1.15. The colours indicate different incidence angles.

The dependence of CPD values on the density is shown in **Figure 3**, where a 10 m one-way penetration depth into firn is modelled at L band with an axial ratio DA of the modelled ice particles of 1.15. This corresponds to a maximum $\Delta\varepsilon$ of 0.035. Larger incidence angles lead to larger CPDs because the vertical-to-horizontal anisotropic structure aligns better with the vertical and horizontal polarizations. The largest CPDs are generated for medium densities, when the volume fraction of the ice particles is around 50%, indicating a heterogeneous ice-air mixture, which gives the highest dielectric anisotropy $\Delta\varepsilon$ for a certain anisotropic firn structure. The CPD approaches 0 for very low densities, towards a pure air medium, and very high densities, towards a pure ice medium. This behavior is shifted with increasing incidence angle due to an increasing effect of refraction.
Showing Δε in dependence of the modelled density and anisotropy, see **Figure 4**, reveals that Δε and thus the CPD is stronger influenced by the anisotropy than the density, and that the density dependence increases with anisotropy, whereas isotropic firn would give no sensitivity of the CPD to density.

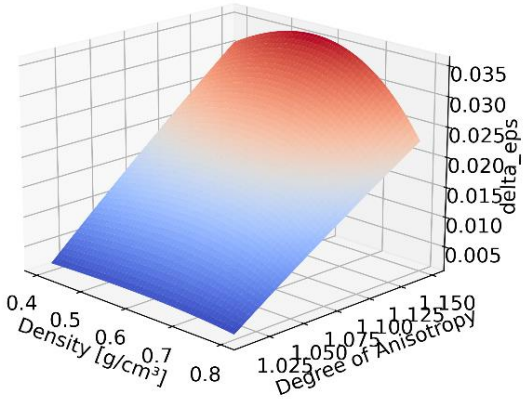

Figure 4 $\sqrt{\varepsilon_H} - \sqrt{\varepsilon_V}$ as a function of anisotropy and density, showing that the dependence on anisotropy is clearly stronger than on density.

2.3 Combination of polarimetric and interferometric phase measurements

The inversion of density, without making assumptions about the vertical backscattering distribution and anisotropy, by means of combining polarimetric and interferometric measurements is analysed.
In a first experiment, an estimation of firn density was attempted by integrating TomoSAR vertical scattering profiles $\sigma_{tomo}(z, \sqrt{\varepsilon_r})$ into the depth-integral of the PolSAR CPD model in (5) [22]. This allows an explicit consideration of backscattering distributions at HH and VV and their respective dependence on $\sqrt{\varepsilon_H}$ and $\sqrt{\varepsilon_V}$. Now, the modelled dielectric anisotropy does not only influence the anisotropic propagation term, but also the depth scaling of the vertical backscattering distribution, as explained in Section 2.1.

$$CPD = \angle\left\{\int_0^l \sigma_{tomo_{HH}}\left(z, \sqrt{\varepsilon_H}\right) e^{-2j\frac{2\pi}{\lambda_0}\sqrt{\varepsilon_H}\frac{z}{\cos\vartheta_r}} \left(\sigma_{tomo_{VV}}\left(z, \sqrt{\varepsilon_V}\right) e^{-2j\frac{2\pi}{\lambda_0}\sqrt{\varepsilon_V}\frac{z}{\cos\vartheta_r}}\right)^* dz\right\} \quad (6)$$

The remaining two unknowns are $\sqrt{\varepsilon_H}$ and $\sqrt{\varepsilon_V}$, respectively density ρ and anisotropy DA. However, this approach is in an early experimental stage with certain limitations. The density inversion can only provide a bulk value for the depth range of the signal penetration and measurements at several incidence angles are required to achieve a non-ambiguous solution. Further, the combined sensitivity to density was not yet analyzed. It also remains to be investigated how the tomographic vertical resolution influences the retrieval of a bulk density and whether (Pol-)InSAR inversions of simple structure models may suffice. Theoretically, a single-baseline inversion of a Uniform Volume structure function would be enough to have an estimate of $\sigma_v\left(z, \sqrt{\varepsilon_{H,V}}\right)$.
The integration of tomographic profiles, or structure model inversions, into the CPD model reduces the number of unknowns to two. Therefore, incidence angle variety is still required to solve for density.

2.4 Incidence angle variation to solve density dependence

In (5) and (6), the dependency of the CPD on the (refracted) incidence angle results in larger phase differences at larger incidence angles, which is shown in **Figure 5** (which is a different slice through the parameter space than in Figure 3). This is because the dielectric anisotropy is between the vertical and horizontal direction and it becomes more effective when the V polarization tends to align more parallel with the vertical.
The incidence angle dependence can be used to solve for density. In case of only polarimetric measurements and employing (5) and modelling the dielectric anisotropy with spheroidal ice inclusions in air, three measurements at different incidence angles are theoretically sufficient to solve

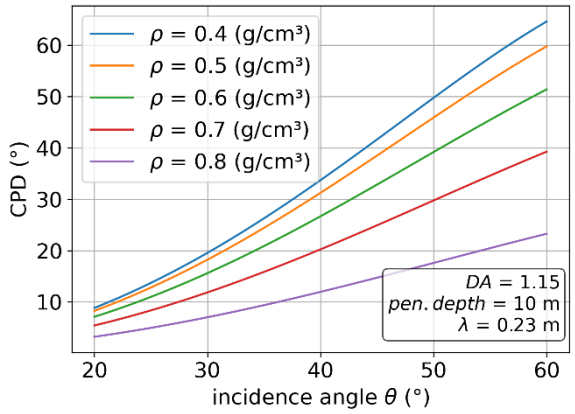

Figure 5 Modelled CPD for an L-band wavelength as a function of incidence angle, for a 10 m one-way penetration depth in anisotropic firn with an axial ratio of the modelled firn grains of 1.15. The colours indicate different densities.

for the three unknowns density, anisotropy and vertical backscattering structure [23]. This requires a very simple single-parameter model for $\sigma(z)$. Extending the PolSAR-only concept of [23] and including tomographic data, as described in Section 2.3, the resulting set of equations for measurements at various incidence angles, can be used to resolve the remaining two unknowns ρ, DA.

$$\begin{aligned} CPD_1 &= CPD_{\theta_1} = f\left(\rho,\ DA, \sigma_{tomo_1}\right) \\ CPD_2 &= CPD_{\theta_2} = f\left(\rho,\ DA, \sigma_{tomo_2}\right) \\ &\dots \\ CPD_n &= CPD_{\theta_n} = f\left(\rho,\ DA, \sigma_{tomo_n}\right) \end{aligned} \tag{7}$$

3 Test site and data

First results are based on airborne experimental SAR data from the percolation zone of Greenland (South Dome location) [7], where the firn in the subsurface is several tens of meters thick and deeper than the L-band signal penetration. **Figure 6** shows the horizontal homogeneity of the area by means of a polarimetric Pauli image (HH+VV blue, HH-VV red, HV green). The location of in situ GNSS measurements is indicated. CPD measurements along these GNSS samples are shown in **Figure 7 (top)** together with the corresponding incidence angle. Their relationship, which highlights also the variability in the CPDs, is shown in **Figure 7 (bottom).** In comparison to **Figure 5**, it becomes evident that the variance in the CPD measurements will complicate a density retrieval.

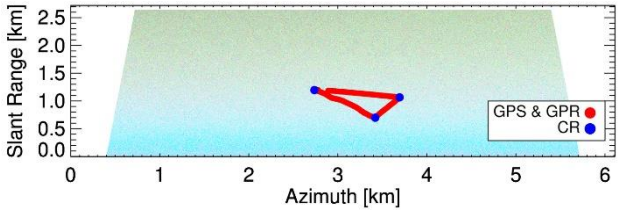

Figure 6 Location of the GNSS track in the center of an airborne polarimetric L-band image from the South Dome test site in Greenland.

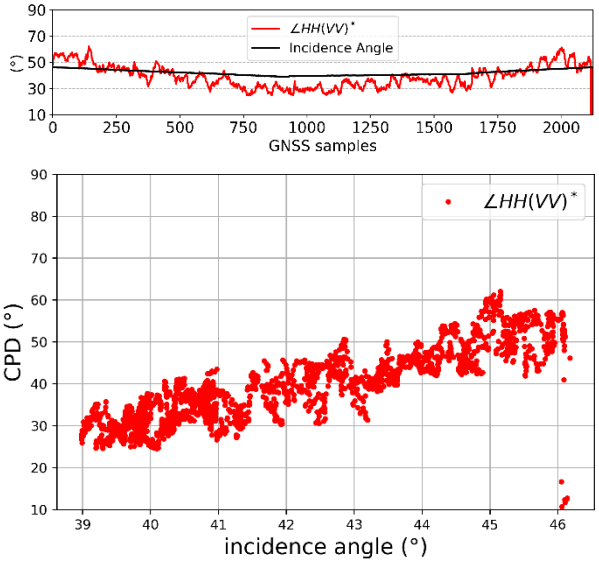

Figure 7 CPD at L-band and incidence angle at the South Dome test site. TOP: along the GNSS track. BOTTOM: CPD vs. incidence angle.

4 First results

A first experiment towards a density retrieval was achieved with a brute force approach by numerically deriving a best fit based on an RMSE between all measured CPDs at the incidence angles along the GNSS track and modelled CPDs, see (7), using the tomographic profiles as described in (6). First results were promising [22] and showed a certain agreement with firn core densities, but the corresponding cost functions of the numerical inversion show only a weak sensitivity to density, see **Figure 8**.

Future research will further investigate the sensitivity to density of this approach and what the impact of the combination of polarimetric and interferometric measurements is, based on simulations and the experimental airborne data. Of interest are the required incidence angle diversity and the required complexity or accuracy of the vertical backscattering distribution.

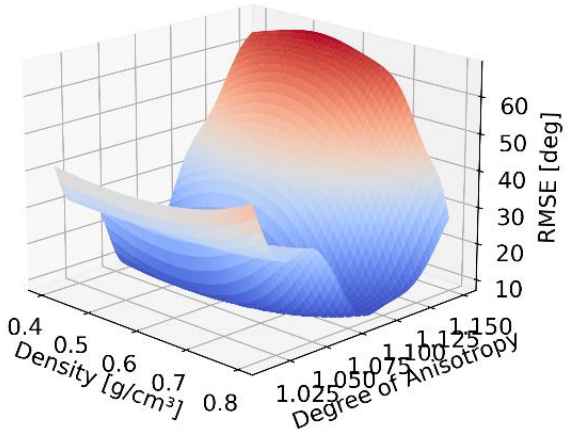

Figure 8 Cost function of the numerical density inversion, which is an RMSE between the measured CPD at various incidence angles and the tomo-supported modelled CPD.

5 Conclusion and Outlook

This study investigates the sensitivity of polarimetric and (multi-baseline) interferometric SAR measurements to the density of snow, firn and ice in the subsurface of ice sheets. Previous studies have shown potential density retrievals based on PolSAR or InSAR measurements at multiple incidence angles separately. Their combination reduces the number of unknowns and could improve the sensitivity to density or reduce the accuracy requirements of the phase measurements. A first sensitivity analysis with respect to density and incidence angle shows the potential, but also the challenging and rather limited sensitivity. Further sensitivity analyses of model and acquisition parameters will lead to a better understanding of the retrieval potential. Future research will address if tomographic profiles are actually required for a bulk density retrieval or to which extent smaller interferometric observation spaces are sufficient.

The possibility of solving the remaining two unknowns in the PolSAR CPD model by combination with TomoSAR profiles was shown. Future work will address if two measurements at different incidence angles would be enough and which incidence angle variability is required. Remembering the permittivity and thus density dependence of a scatterer's location within the subsurface, see (3), a second measurement from a different incidence angle gives a system of two equations and two unknowns also in a pure InSAR case. Therefore, future work will investigate how the inclusion of polarimetric phase measurements influences the sensitivity to density and the accuracy requirements.

Finally, the density estimates have to be interpreted carefully, since the underlying models are (strong) approximations of the real firn structure. This could be addressed in the future by an integration with firn densification models.

6 Literature

[1] D.G. Vaughan et al., "Observations: Cryosphere," in Climate Change 2013: The Physical Science Basis. Contribution of Working Group I to the Fifth Assessment Report of the Intergovernmental Panel on Climate Change, [Stocker, T.F. et al. (eds.)]. Cambridge University Press, Cambridge, United Kingdom and New York, USA, 2013.

[2] K. Shahateet, T. Seehaus, F. Navarro, C. Sommer, and M. Braun, "Geodetic Mass Balance of the South Shetland Islands Ice Caps, Antarctica, from Differencing TanDEM-X DEMs," Remote Sensing, vol. 13, no. 17, p. 3408, Aug. 2021, doi: 10.3390/rs13173408.

[3] F. J. Navarro, U. Y. Jonsell, M. I. Corcuera, and A. Martín-Español, "Decelerated mass loss of Hurd and Johnsons Glaciers, Livingston Island, Antarctic Peninsula," J. Glaciol., vol. 59, no. 213, pp. 115–128, 2013, doi: 10.3189/2013JoG12J144.

[4] M. Huss, "Density assumptions for converting geodetic glacier volume change to mass change," The Cryosphere, vol. 7, no. 3, pp. 877–887, May 2013, doi: 10.5194/tc-7-877-2013.

[5] E. Rignot, K. Echelmeyer, and W. Krabill, "Penetration depth of interferometric synthetic-aperture radar signals in snow and ice," Geophysical Research Letters, vol. 28, no. 18, Art. no. 18, Sep. 2001, doi: 10.1029/2000GL012484.

[6] L. Tsang et al., "Review article: Global monitoring of snow water equivalent using high-frequency radar remote sensing," The Cryosphere, vol. 16, no. 9, pp. 3531–3573, Sep. 2022, doi: 10.5194/tc-16-3531-2022.

[7] G. Fischer, K. P. Papathanassiou and I. Hajnsek, "Modeling Multifrequency Pol-InSAR Data from the Percolation Zone of the Greenland Ice Sheet," IEEE Transactions on Geoscience and Remote Sensing, vol. 57, no. 4, pp. 1963-1976, 2019.

[8] J. Sharma, I. Hajnsek, K.P. Papathanassiou, and A. Moreira, "Estimation of glacier ice extinction using long-wavelength airborne Pol-InSAR," IEEE Transactions on Geoscience and Remote Sensing, vol. 51, no. 6, pp. 3715-3732, Jun. 2013.

[9] S. Tebaldini, T. Nagler, H. Rott, and A. Heilig, "Imaging the Internal Structure of an Alpine Glacier via L-Band Airborne SAR Tomography," IEEE Transactions on Geoscience and Remote Sensing, vol. 54, no. 12, pp. 7197–7209, 2016.

[10] F. Banda, J. Dall, and S. Tebaldini, "Single and Multipolarimetric P-Band SAR Tomography of Subsurface Ice Structure," IEEE Transactions on Geoscience and Remote Sensing, vol. 54, no. 5, pp. 2832–2845, 2016.

[11] M. Pardini, G. Parrella, G. Fischer, and K. Papathanassiou, "A Multi-Frequency SAR Tomographic Characterization of Sub-Surface Ice Volumes," in Proceedings of EUSAR, Hamburg, Germany, 2016.

[12] G. Parrella, I. Hajnsek, and K. P. Papathanassiou, "Retrieval of Firn Thickness by Means of Polarisation Phase Differences in L-Band SAR Data," Remote Sensing, vol. 13, no. 21, p. 4448, Nov. 2021, doi: 10.3390/rs13214448.

[13] C. Matzler, "Microwave permittivity of dry snow," IEEE Trans. Geosci. Remote Sensing, vol. 34, no. 2, pp. 573–581, Mar. 1996, doi: 10.1109/36.485133.

[14] B. Rekioua, M. Davy, L. Ferro-Famil, and S. Tebaldini, "Snowpack permittivity profile retrieval from tomographic SAR data," Comptes Rendus Physique, vol. 18, no. 1, Art. no. 1, Jan. 2017, doi: 10.1016/j.crhy.2015.12.016.

[15] X. Xu, C. A. Baldi, J.-W. De Bleser, Y. Lei, S. Yueh, and D. Esteban-Fernandez, "Multi-Frequency Tomography Radar Observations of Snow Stratigraphy at Fraser During SnowEx," in IGARSS 2018 - 2018 IEEE International Geoscience and Remote Sensing Symposium, Valencia: IEEE, Jul. 2018, pp. 6269–6272. doi: 10.1109/IGARSS.2018.8519538.

[16] O. Frey, C. L. Werner, R. Caduff, and A. Wiesmann, "Inversion of SNOW structure parameters from time series of tomographic measurements with SnowScat," in 2017 IEEE International Geoscience and Remote Sensing Symposium (IGARSS), Fort Worth, TX: IEEE, Jul. 2017, pp. 2472–2475. doi: 10.1109/IGARSS.2017.8127494.

[17] S. Tebaldini, L. Ferro-Famil, D. Giudici, and F. Banda, “An Investigation of Snow Water Equivalent Retrieval by Across-Track SAR Formations,” in ESA POLinSAR Workshop, Toulouse, France, 2023.

[18] L. Ferro-Famil, S. Tebaldini, M. Davy, and F. Boute, “3D SAR imaging of the snowpack in presence of propagation velocity changes: Results from the Alp-SAR campaign,” IEEE, Jul. 2014, pp. 3370–3373. doi: 10.1109/IGARSS.2014.6947203.

[19] G. Fischer, M. Jäger, K. P. Papathanassiou, and I. Hajnsek, “Modeling the Vertical Backscattering Distribution in the Percolation Zone of the Greenland Ice Sheet with SAR Tomography,” accepted for publication in IEEE Journal of Selected Topics in Applied Earth Observations and Remote Sensing, October 2019.

[20] G. Parrella, I. Hajnsek and K. P. Papathanassiou, "On the Interpretation of Polarimetric Phase Differences in SAR Data Over Land Ice," in IEEE Geoscience and Remote Sensing Letters, vol. 13, no. 2, pp. 192-196, 2016.

[21] S. Fujita et al., “Densification of layered firn of the ice sheet at NEEM, Greenland,” Journal of Glaciology, vol. 60, no. 223, Art. no. 223, 2014, doi: 10.3189/2014JoG14J006.

[22] G. Fischer, K. Papathanassiou, I. Hajnsek, and G. Parrella, “Combining PolSAR, Pol-InSAR and TomoSAR for Snow and Ice Subsurface Characterization,” presented at the ESA POLinSAR Workshop, Online, Apr. 2021.

[23] G. Parrella, I. Hajnsek, and K. Papathanassiou, “Estimation of snow and firn properties by means of multi-angular polarimetric SAR measurements,” in European Conference on Synthetic Aperture Radar (EUSAR), VDE, Apr. 2021. [Online]. Available: https://elib.dlr.de/133993/